Taylor & Francis
Taylor & Francis Group

# RESEARCH ARTICLE

## HF ground wave propagation over a curved rough sea surface in the presence of islands

C. Bourlier[a]* and G. Kubické[b]

[a]*IREENA, Polytech'Nantes-Université de Nantes, La Chantrerie, Rue C. Pauc, 44306 Nantes Cedex 3, BP 50609, France; [b]DGA-MI (Direction Générale de l'Armement – Direction Technique – Maitrise de l'Information), CGN1 division, 35170 Bruz, France*

For a vertically polarized line source, in the context of HF (3–30 MHz) ground wave propagation over a curved rough sea surface in the presence of islands, this paper adapts the FB-SA (Forward–Backward Spectral Acceleration) method to compute the attenuation function over sea–land (island)–sea mixed paths for different shapes and heights of the islands. The rigorous FB-SA numerical method is based on the method of moments and was originally developed for scattering from rough surfaces and is especially efficient in solving a huge problem, which is required to predict the ground wave propagation over a long surface. In addition, for zero island height, this method is compared with an analytical approach expressed from a (residue) series, in which the roots of a differential equation, depending on the Airy function, must be calculated. In addition, from an intuitive approach and from the work of Barrick and Ishimaru, this analytical approach is extended to include the sea roughness and then validated from the FB-SA.

## 1. Introduction

There are many problems in communications, navigation, and applied geophysics, in which the system performance is dependent on the electromagnetic ground wave. The latter refers to the wave that propagates along the surface of the Earth such that its characteristics are influenced by the profile and electrical properties of the Earth's surface. In the last century, much effort was undertaken to solve this issue. For a complete review of this problem, see the papers of Collin [1], for a *homogeneous flat* surface, and of Wait [2] and Sevgi and Apaydin [3,4] for an *inhomogeneous curved* surface. Also read the references quoted in these reviews. In these papers, the sea roughness effect is not investigated.

Recently, Bourlier et al. [5–7] thoroughly studied the ground wave propagation over a one-dimensional surface. In [5], the Earth is assumed to be flat, whereas in [6], the curvature of the Earth is taken into account, and in [7] the Earth is assumed to be flat like [5], but the permittivity of the surface varies along its abscissa (this case will

---

*Corresponding author. Email: christophe.bourlier@univ-nantes.fr

2                                *C. Bourlier and G. Kubické*

be referred as an inhomogeneous surface) allowing the authors to compute the ground wave over sea–land–sea mixed paths. In addition, in these papers, from an
40    intuitive approach based on the work of Barrick [8,9] and Ishimaru [10], the sea roughness is taken into account from an asymptotic analytical approach. Then, good agreement is obtained between the intuitive approach and a rigorous method (BMIA-CAG [11–13] for a flat surface and FB-SA [14–18] for a curved surface) taken as a reference.
45        The purpose of this paper is to extend the previous studies of Bourlier et al. to a curved rough surface in the presence of islands, to predict, for instance, the attenuation function over sea–land–sea mixed curved paths, in which the roughness is taken into account for the sea. The reference rigorous method applied in this paper is the FB-SA. It was obtained from the boundary integral equations and solved by
50    the method of moments (MoM), in which two procedures of acceleration are involved, FB (Forward–Backward) and SA (Spectral Acceleration), which makes the method very efficient. Indeed, its complexity is then $\mathcal{O}(N)$ ($N$ is the number of unknowns on the surface), instead of $\mathcal{O}(N^3)$ from a direct LU inversion, and the memory storage is significantly reduced ($\mathcal{O}(N)$) in comparison to a direct LU
55    inversion ($\mathcal{O}(N^2)$). In addition, in this paper, to our knowledge, this is the first time that the sea roughness effect has been investigated both from analytical asymptotic (cf. the work of Feinberg [19] and Barrick [8,9]) and rigorous (FB-SA) methods. Then, the FB-SA is adapted to a surface, for which its permittivity varies with respect to its abscissa (inhomogeneous surface).
60        Other recent work, like [3,4], treated essentially the same problem using a completely different rigorous numerical method. It is based on a finite element method (FEM). The advantage of the FEM is to be able to model an atmospheric refractivity variation (duct). Their algorithm is then compared with the results computed from the Millington curve fitting method [20,21], tested in [22].
65    In comparison to the FEM, the FB-SA does not account for the duct effect but treats the roughness easily. Nevertheless, for a linear profile of the refractive index of air, the FB-SA can always be applied by modifying the Earth's radius.
        The paper is organized as follows. Section 2 presents the analytical solution of the ground wave propagation above a smooth curved surface made up of three zones of
70    different permittivities. In Section 3, the FB-SA method is briefly presented and adapted to a surface, for which its permittivity varies with respect to its abscissa. In Section 4, the analytical solution is compared with the FB-SA by taking the sea surface roughness into account, and numerical results obtained from the FB-SA are also presented for different shapes of island. The last section gives concluding
75    remarks. The $e^{-j\omega t}$ time convention is assumed.

## 2. Analytical asymptotic solution

This section presents a closed-form expression of the attenuation function for the ground wave propagation above a smooth curved surface made up of three zones of different permittivities, obeying a parabolic profile ($z_E(x) = -x^2/(2a)$) where $a$ is the

80 Earth's radius) and assumed to be highly conducting. We adopt the notation used by Bremmer [23].

For a surface made up of three zones of different permittivies, the attenuation function $F = \psi/(2\psi_i)$, in which $\psi$ is the total field and $\psi_i$ the incident field of a line source, is expressed as [19]

$$F(x) = \begin{cases} F_1(x) & \text{for } x \in [0; d_1[ \\ F_2(x) & \text{for } x \in [d_1; d_1 + d_2[ \\ F_3(x) & \text{for } x \in [d_1 + d_2; d_1 + d_2 + d_3[. \end{cases} \tag{1}$$

85 For a surface of constant permittivity ($x \in [0; d_1[$ in Figure 1), the attenuation function is [23]

$$F_{1,M_1}(x) = (k_0 a)^{\frac{1}{6}} \left(\frac{2\pi j x}{a}\right)^{\frac{1}{2}} \sum_{m_1=1}^{m_1=M_1} G_{m_1}(v_0) G_{m_1}(v) \frac{\exp\left[\frac{j(k_0 a)^{\frac{1}{3}} x \tau_{m_1}}{a}\right]}{2\tau_{m_1} - \frac{1}{\delta_1^2}}, \tag{2}$$

where

$$\delta_1 = \frac{j}{\Delta_1 (a k_0)^{\frac{1}{3}}}, \tag{3}$$

and

$$G_{m_1}(v) = \frac{w(\tau_{m_1} - v)}{w(\tau_{m_1})}, \quad v_0 = \frac{k_0 z_0}{(k_0 a)^{1/3}}, \quad v = \frac{k_0 z}{(k_0 a)^{1/3}}. \tag{4}$$
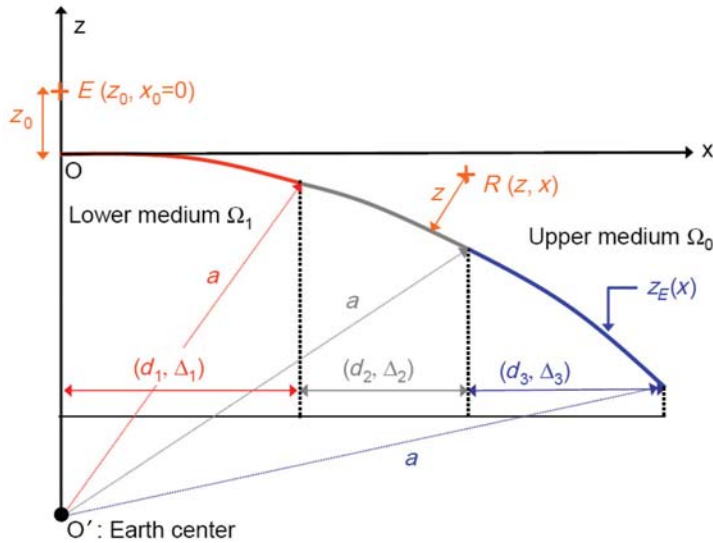


Figure 1. Curved surface of constant radius $a$ and of horizontal length $d_1 + d_2 + d_3$ made up of three sections of lengths $\{d_1, d_2, d_3\}$ and of surface normalized impedances $\{\Delta_1, \Delta_2, \Delta_3\}$.

4                                    *C. Bourlier and G. Kubické*

From Equation (2), the attenuation function is then $F_1(x) = \lim_{M_1 \to \infty} F_{1,M_1}(x)$.
$k_0 = 2\pi/\lambda_0$ is the incident wavenumber of the upper medium assumed to be vacuum
and $a = 6378$ km is the maximum equatorial radius of the Earth.

The function $G_{m_1}$ is a "height-gain" function, in which $z_0$ is the emitter height and
$z$ the receiver height (see Figure 1). The surface is assumed to be highly conducting
($|\Delta_1| \ll 1$ or $|n_1| \gg 1$) and $\Delta_1 \approx 1/n_1$ is the surface normalized impedance of the first
path, in which $n_1$ is the refractive index of the surface. Thus, the Leontovitch
boundary condition can be applied. In addition, $\{\tau_{m_1}\}$ are the roots of the following
equation

$$w'(\xi) - q_1 w(\xi) = 0, \quad q_1 = -\frac{1}{\delta_1 2^{\frac{1}{3}}}, \quad \xi = 2^{\frac{1}{3}}\tau, \tag{5}$$

where $w(\xi) = \text{Bi}(\xi) + j\text{Ai}(\xi)$ is expressed in terms of the Airy functions. The sum (2)
converges if the roots $\tau_{m_1}$ are ordered as $-\text{Im}(\tau_1) > -\text{Im}(\tau_2) > \cdots > -\text{Im}(\tau_{M_1})$,
where the symbol Im stands for the imaginary part, and $M_1$ is the number of roots.
Among a number of different algorithms to determine the roots $\{\tau_n\}$, the one
described in [24] (pp. 340–343) is efficient and valid for a wide range of frequencies
and ground constants. Its principle is summarized and tested in Appendix B of [6].
An analytical series expansion of $\tau_{m_1}$ can be also found in [25].

From numerical simulations, the number of roots (i.e. modes in terms of Airy
functions) drastically increases near to the transmitter (it can reach 10,000 and
more). On the other hand, the lowest 1–3 roots (dominant mode and a few others)
are enough at long range in the shadow region. Typically, we take a number of
modes varying between 50 and 100 and this number decreases as $|\Delta_i|$ and/or the
frequency increases.

In Figure 1, for $x \in [d_1; d_1 + d_2[$, the attenuation function is expressed as [19]

$$F_{2,M_1,M_2}(x) = (k_0 a)^{\frac{1}{6}} \left(\frac{2\pi jx}{a}\right)^{\frac{1}{2}} 2^{\frac{2}{3}} \sum_{m_1=1}^{m_1=M_1} \sum_{m_2=1}^{m_2=M_2} G_{m_1}(v_0) G_{m_2}(v)$$
$$\times \frac{\exp\left\{\frac{j(k_0 a)^{\frac{1}{3}}[\tau_{m_1}d_1 + \tau_{m_2}(x-d_1)]}{a}\right\}}{\left(\tau_{m_1} - \tau_{m_2}\right)\left(2\tau_{m_1} - \frac{1}{\delta_1^2}\right)\left(2\tau_{m_2} - \frac{1}{\delta_2^2}\right)}, \tag{6}$$

and $F_2(x) = \lim_{M_1 \to \infty, M_2 \to \infty} [F_{2,M_1,M_2}(x)]$.

In Figure 1, for $x \in [d_1 + d_2; d_1 + d_2 + d_3[$, the attenuation function is expressed
as [19]

$$F_{3,M_1,M_2,M_3}(x) = (k_0 a)^{\frac{1}{6}} \left(\frac{2\pi jx}{a}\right)^{\frac{1}{2}} 2^{\frac{4}{3}} \sum_{m_1=1}^{m_1=M_1} \sum_{m_2=1}^{m_2=M_2} \sum_{m_3=1}^{m_3=M_3} G_{m_1}(v_0) G_{m_3}(v)$$
$$\times \frac{\exp\left\{\frac{j(k_0 a)^{\frac{1}{3}}[\tau_{m_1}d_1 + \tau_{m_2}(d_2-d_1) + \tau_{m_3}(x-d_2)]}{a}\right\}}{\left(\tau_{m_1} - \tau_{m_2}\right)\left(\tau_{m_2} - \tau_{m_3}\right)\left(2\tau_{m_1} - \frac{1}{\delta_1^2}\right)\left(2\tau_{m_2} - \frac{1}{\delta_2^2}\right)\left(2\tau_{m_3} - \frac{1}{\delta_3^2}\right)}, \tag{7}$$

115 and $F_3(x) = \lim_{M_1 \to \infty, M_2 \to \infty, M_3 \to \infty} \left[ F_{3,M_1,M_2,M_3}(x) \right]$.

For each section, $i = \{1, 2, 3\}$, the roots $\{\tau_{m_i}\}$ are again obtained from Equation (5) by replacing the subscript "1" by "$i$".

Equations (2), (6) and (7) show that the addition of a section does not disturb the scattered field by the previous sections and that for each new section, an additional
120 sum appears, which makes the evaluation of the sums more complex.

In the following, the surface complex relative permittivity $\epsilon_{ri}$ of section $i$ is assumed to be

$$\epsilon_{ri} = \epsilon_{ri}' + \frac{j\sigma_i}{2\pi f \epsilon_0} = \epsilon_{ri}' + \frac{18 j \sigma_i}{f \, (\text{GHz})}, \tag{8}$$

where $\sigma_i$ is the conductivity in S/m and $n_i = \sqrt{\epsilon_{ri}}$. For the sea surface ($i = \{1, 3\}$), $\sigma_i = 4$ S/m and the real part of the relative permittivity is $\epsilon_{ri}' = 80$, which implies that
125 the complex relative permittivity of the sea is $\epsilon_{ri} = 80 + 72j/f$, with $f$ in GHz. For instance, for $f = 10$ MHz, $\epsilon_{ri} = 80 + j7200$. In addition, for the island ($i = 2$), $(\epsilon_{ri}', \sigma_i) = (30, 0.01 \text{ S/m})$, corresponding to a very wet soil.

## 3. Rigorous numerical method

For a surface of constant permittivity, Bremmer [23] and Feinberg [19] started from
130 the scalar integral equation of a 2-D surface, converted into a single integral from a saddle point approximation. Bourlier et al. [6] then showed that the integral equation satisfied by the attenuation function and derived from a 1-D surface is exactly the same as that obtained in the papers of Bremmer and Feinberg. Thus, for the reference rigorous method, the surface can be assumed to be 1-D.
135 This section presents and tests the rigorous FB-SA fast method.

### 3.1. *Introduction*

The FB-SA method allows us to consider a huge problem. Indeed, to exhibit the ground wave, which propagates near the surface far from the transmitter, the surface must be very long, typically, a few hundred kilometers. For a frequency of the order
140 of 10 MHz ($\lambda_0 = 30$ m) and with a sampling step of $\lambda_0/10 = 3$ m, the number of unknowns on the surface must then be greater than $N = 100,000$.

The principle of the FB-SA is not to invert the impedance matrix $\bar{\mathbf{Z}}$, obtained from the discretization of the integral equations by the MoM, but to replace $\bar{\mathbf{Z}}^{-1}\mathbf{b}$, in which the vector $\mathbf{b}$ is related to the incident field, by a succession of matrix-vector
145 products. Two procedures of acceleration are then involved: the FB (Forward–Backward) and the SA (Spectral Acceleration), which makes the method very efficient. Indeed, its complexity is then $\mathcal{O}(N)$ ($N$ is the number of unknowns on the surface) and the memory storage is significantly reduced in comparison to a direct LU inversion. For more details, see [14–18].
150 In this paper, the FB-SA is updated by considering that the relative permittivity of the lower medium $\Omega_1$ (see Figure 1), $\epsilon_r(x)$, varies along the horizontal distance $x$. Under the IBC (Impedance Boundary Condition also named the Leontovitch

6                                    *C. Bourlier and G. Kubické*

boundary condition) approximation, the skin depth $\delta_i = \lambda_0/[2\pi \text{Im}(n_i)]$ of a section $i$ is much smaller than the incident wavelength $\lambda_0$ because $|\text{Im}(n_i)| \gg 1$. In the lower
155    medium $\Omega_1$, the field then damps very strongly with respect to the vertical $z$. Thus, we assume in $\Omega_1$ that the scattered fields of each section $i$ of constant relative permittivity $\epsilon_{ri}$ do not interact between them. Considering this assumption, the impedance matrix of the MoM is modified and we have made some changes in the algorithm of the FB-SA to take into account the fact that $\epsilon_r(x)$ is a function of $x$.
160    For the TM polarization, the use of IBC leads to $\partial \psi(\mathbf{r}')/\partial n_s = -j\Delta_i k_0 \psi(\mathbf{r}')$ on the surface, where $\psi(\mathbf{r}')$ is the field on the surface and $\partial \psi(\mathbf{r}')/\partial n_s$ its normal derivative. The scattered field, $\psi_s$, is then computed by applying the Huygens principle defined as

$$\psi_s(\mathbf{r}) = \int_S \left[ \frac{\partial g_0(\mathbf{r}', \mathbf{r})}{\partial n_s} \psi(\mathbf{r}') - \frac{\partial \psi(\mathbf{r}')}{\partial n_s} g_0(\mathbf{r}', \mathbf{r}) \right] \mathrm{d}S'. \tag{9}$$

The function $g_0$ is the scalar Green function. To be consistent with Equations (2), (6)
165    and (7), for the computation of the scattered field $\psi_s$, $\mathbf{r} = (x, z)$ must be expressed in the coordinate system of the Earth, leading to the following changes

$$\begin{cases} x \rightarrow x - z \sin\alpha \\ z \rightarrow z_E + z \cos\alpha \end{cases} \quad \alpha = \tan\left(\frac{\partial z_E}{\partial x}\right) = -\tan\left(\frac{x}{\sqrt{a^2 - x^2}}\right), \tag{10}$$

for a circular profile of the Earth ($z_E(x) = -a + \sqrt{a^2 - x^2}$).

The attenuation function is then computed from $\psi_s$ as

$$F(\mathbf{r}) = \frac{\psi_s(\mathbf{r}) + \psi_i(\mathbf{r})}{2\psi_i(\mathbf{r})} = F(x, z), \tag{11}$$

where the incident field $\psi_i(\mathbf{r})$ (line source of amplitude 1 V/m) is defined as

$$\psi_i(\mathbf{r}) = g_0(\mathbf{r}, \mathbf{r}_0) = \frac{j}{4} H_0^{(1)}\left( k_0 \sqrt{(x - x_0)^2 + (z - z_0)^2} \right), \tag{12}$$

170    in which $H_0^{(1)}$ is the Hankel function of zero order and first kind.

The surface length is $L = N\lambda_0/10$ ($x \in [-L/2; L/2]$), since the sampling step is $\lambda_0/10$. It should be noted that $x_{\max} = \max(x) = N\lambda_0/20$.

### 3.2. *Numerical tests*

From small surface lengths, in this subsection the attenuation function computed
175    from the FB-SA is compared with that computed from a direct LU inversion. The frequency is $f = 10\,\text{MHz}$ and the number of unknowns on the surface is $N = 10,000$, corresponding to a surface length of 30 km. In order to have a significant effect on the surface curvature, the Earth's radius is artificially decreased, such that $a$ becomes $0.06 \times a = 383$ km.
180    Although the FB-SA can be applied to arbitrary irregular terrain profiles and following the same procedure as in [3,4], in this paper three analytical shapes of islands are considered. A Gaussian (label "Gau"), a half-cosinusoidal (label "H-c")

and Circular (label "Cir") shapes defined for $x \in [x_1 - w_1/2; \, x_1 + w_1/2]$ in the island local basis by

$$z_1(x) = \begin{cases} h_1 \exp\left(-\left[\dfrac{x - x_1}{w_1/2}\right]^2\right) & \text{(Gau)} \\[2ex] h_1 \cos\left(\dfrac{\pi[x - x_1]}{w_1}\right) & \text{(H-c)} \\[2ex] z_1(x) = h_1\sqrt{1 - \left(\dfrac{x-x_1}{w_1/2}\right)^2} & \text{(Cir)} \\[2ex] 0 & \text{(Nul)} \end{cases} \tag{13}$$

185 where $h_1$ is the maximum height of the island, $w_1$ its width and $x_1$ its center. The label "Nul" means that the island height is zero. One can verify that $z_1(x_1 \pm w_1/2) \approx 0$ to avoid any height discontinuity with the adjacent sections.

The left part of Figure 2 shows the profiles versus the abscissa for sea–land–sea mixed smooth paths. The center of the island is $x_1 = 0$ and for the emitter, 190 $x_0 = -10$ km, $z_0 = 5$ m. The right part of Figure 2 shows the corresponding ratio $|F^{\mathrm{FBSA}}/F^{\mathrm{LU}}|$, in dB scale, computed for a receiver height $z = 5$ m. $F^{\mathrm{FBSA}}$ is the attenuation function computed from the FB-SA, whereas $F^{\mathrm{LU}}$ is computed from a direct LU inversion. The strong interaction distance of the FB-SA is $x^{\mathrm{FBSA}} = 50\lambda_0 = 1500$ m for $z_1 = 0$, whereas $x^{\mathrm{FBSA}} = 150\lambda_0 = 4500$ m for $z_1 \neq 0$. Moreover, the 195 iteration number of FB is $N^{\mathrm{FBSA}} = 3$.

As we can see, the attenuation function $F^{\mathrm{FBSA}}$ over the first path agrees very well with that computed from a direct LU inversion and, over the second and third paths, a slight disagreement is observed, except for $h_1 = 0$, for which the results match very well. In addition, the difference decreases as the horizontal distance 200 from the island decreases and as the width and the maximum height of the island decrease.

In conclusion, for zero island height, the FB-SA is very efficient (the ratio $|F^{\mathrm{FBSA}}/F^{\mathrm{LU}}|$ does not exceed 0.01 dB), whereas for $z_1 \neq 0$, a slight disagreement occurs between the FB-SA and LU methods (but does not exceed 0.2 dB), 205 and the difference decreases as the horizontal distance from the island increases.

## 4. Numerical results

For the simulations, the surface is assumed to be symmetrical with respect to the origin, which means that $x_0 = 0$ and $x_2 = x - x_0 = x$. This implies that the scattered 210 field is also symmetrical, and thus, the results will be plotted for $x_2 = x \geq 0$. In addition, $N^{\mathrm{FBSA}} = 3$. The surface length is $L = N\lambda_0/10$ ($x \in [-L/2; \, L/2]$), since the sampling step is $\lambda_0/10$. It should be noted that $x_{\max} = \max(x) = N\lambda_0/20$. For instance, for $f = 10$ MHz with $N = 100{,}000$, $x_{\max} = 150$ km.

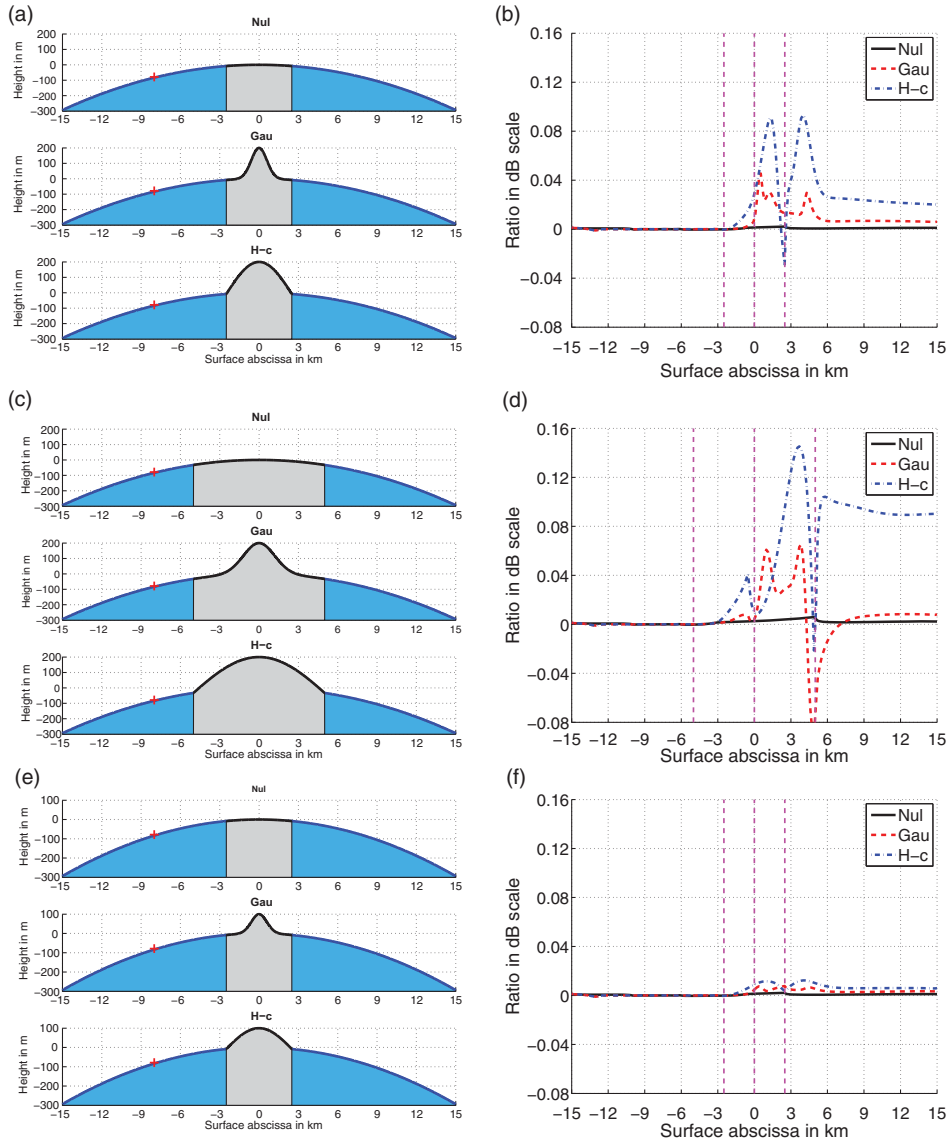8                          *C. Bourlier and G. Kubické*



Figure 2. Left: profiles of the surface versus the abscissa $x$ in km for sea–land–sea mixed smooth paths. The island's center is $x_1 = 0$ and $N = 10,000$. The cross indicates the location of the emitter, for which $x_0 = -10$ km and $z_0 = 5$ m. The different colors means that the permittivity changes. For each title of the subfigures, the label "Nul" means that $h_1 = 0$, the label "Gau" means that the island has a Gaussian shape, and the label "H-c" means that the island has a half-cosinusoidal shape. Right: ratio $|F^{FBSA}/F^{LU}|$ in dB scale versus the abscissa $x$. The vertical lines indicate the beginning, the center and the end of the island. The frequency is $f = 10$ MHz.

### 4.1. *Smooth sea and zero island height*

215  In this subsection, the sea section is assumed to be smooth and the island's maximum height is $h_1 = 0$. In the FB-SA algorithm, the strong interaction distance $x^{\text{FBSA}} = 50\lambda_0$.

Figure 3 plots the modulus of the attenuation function, $|F|$, versus the horizontal distance $x_2 = x - x_0$. For each figure, the simulation parameters are reported in Table 1. In the legend, the label "FBSA" means that the results are computed from
220  the FB-SA, whereas the label "ANAL" means that the results are computed from the analytical asymptotic approach (Feinberg formulation [19], Section II). For Figure 3(a) and (b), $(\epsilon_{r2}, \sigma_2)$ vary (in the legend the label "H" means that the surface is homogeneous, $(\epsilon_{r2}, \sigma_2) = (\epsilon_{r1}, \sigma_1) = (\epsilon_{r3}, \sigma_3)$, whereas the label "I" means that the surface is inhomogeneous). In Figure 3(c), the receiver height varies.
225  Figure 3(d) plots the same variation as in Figure 3(b) but versus $x_2$ and the receiver height $z$ and from the FB-SA. For Figure 3(e), $x_f = x_1 + w_1/2 = 50$ km (the abscissa at the end of the island) is constant, whereas in Figure 3(e), $x_d = x_1 - w_2/1 = 20$ km (the abscissa at the beginning of the island) is constant.

For sea–land–sea mixed paths, Figure 3(a), (b), (e) and (f) show very good
230  agreement between the results computed from the analytical approach and the FB-SA, since the difference remains smaller than 1 dB. As shown in [7], for a *flat* surface, like a *curved* surface, a sharp decrease occurs in the signal strength along the sea–island transition and the signal recovers itself after the island–sea transition (beyond the island) to converge towards the signal obtained for a homogeneous *flat*
235  surface. This phenomenon is known as the Millington (recovery) effect. For an inhomogeneous curved surface, in the shadowed zone (below the line-of-sight), this phenomenon occurs but the signal remains smaller than that obtained from a homogeneous curved surface. From theoretical arguments, this fundamental difference between flat and curved inhomogeneous surfaces was pointed out by
240  Feinberg [19].

For $x$ close to 0 or $d_1$ or $d_1 + d_2$ (the abscissa for which a new section starts), the difference is greater because the number of roots retained for the calculation of the sums is not enough. Indeed, the sum given by Equation (2) converges very slowly for $x$ close to zero. A means to avoid this problem is to express the sums as the
245  convolution product integrals [26] like a flat surface [7], but this is not the purpose of this paper.

Figure 3(c) shows that the height of the receiver has a significant impact on the signal strength above the island (see also Figure 3(d)), for which the analytical approach predicts bad results. On the other hand, above the sea paths, when the
250  receiver height increases, the signal strength weakly decreases and good agreement is observed between both methods. It is important to note that the inclusion of the "height gain" function in Equations (6) and (7) comes from a heuristic approach. This approach is rigorous for only a homogeneous surface (see Equation (2)).

### 4.2. *Rough sea and zero island height*

255  In this subsection, a rough sea surface is considered and $h_1 = 0$. In the FB-SA algorithm, the strong interaction distance is $x^{\text{FBSA}} = 50\lambda_0$.
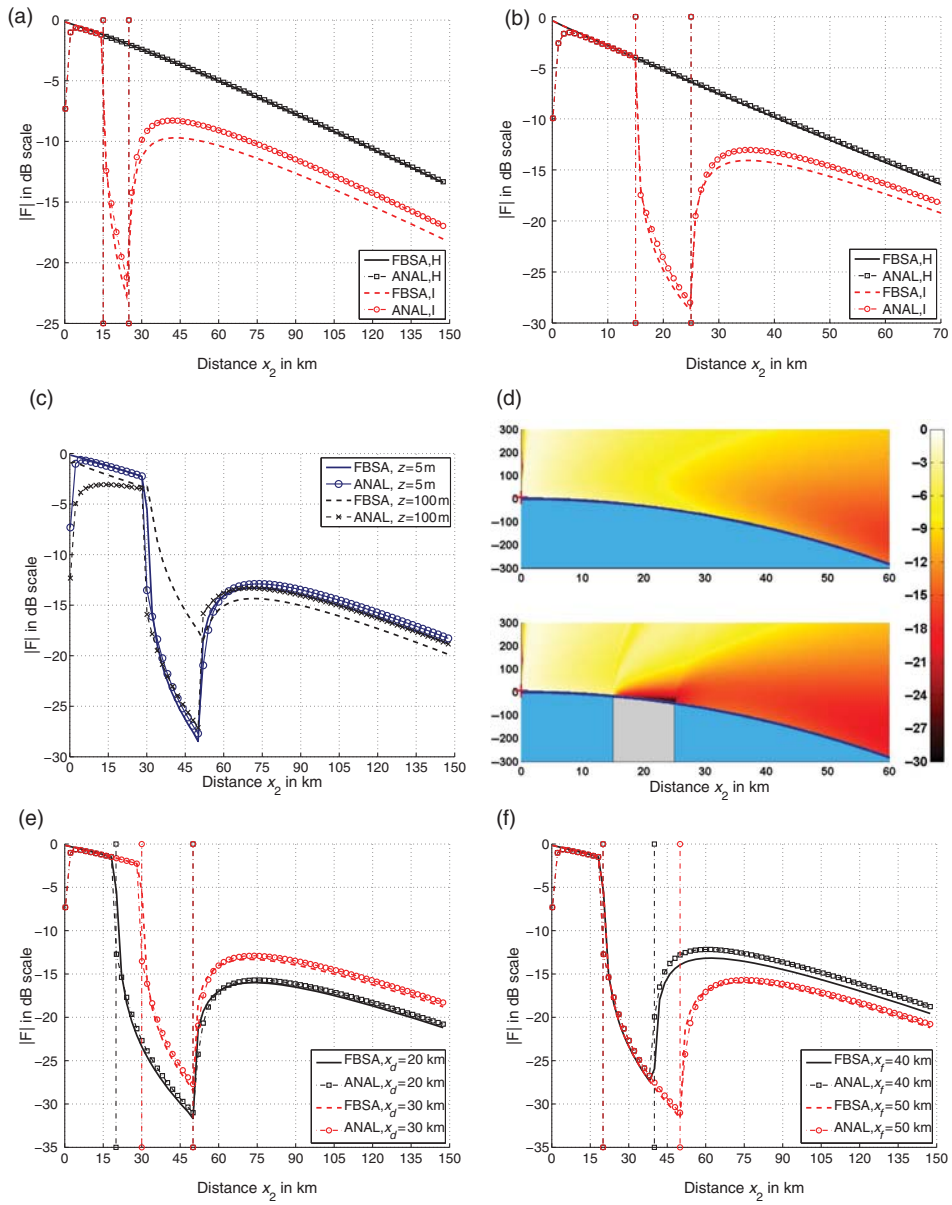
Figure 3.  $|F|$ versus the horizontal distance $x_2 = x - x_0$ in km (and $z$ in m for Figure 3(d)) for a smooth curved surface. The parameters are given in Table 1. The dashed vertical lines indicate the values of the abscissa at the beginning $(x_d)$ and at the end $(x_f)$ of the island.

The rough surface height is assumed to be a Gaussian stationary stochastic process with zero mean value, and the height spectrum obeys the Elfouhaily et al. hydrodynamic spectrum [27], in which the key parameter is the wind speed $u_{10}$ at 10 meters above the sea surface. From an electromagnetic point of view, in the

Table 1. Parameters used for Figures 2–3(f). The wind speed is $u_{10} = 0$ (smooth sea surface), $\epsilon_{r1} = \epsilon_{r3} = 80$, $\sigma_1 = \sigma_3 = 4\,\text{S/m}$, the maximum height of the island is $h_1 = 0$, the height of the emitter is $z_0 = 10\,\text{m}$ and its abscissa is $x_0 = 0\,\text{m}$. The symbol "–" means that the corresponding parameter changes in the figures.

| Figure | $f$ (MHz) | $z$ m | $x_1$ km | $w_1$ km | $(\epsilon_{r2}, \sigma_2)$ (–, S/m) |
|---|---|---|---|---|---|
| 3(a) | 10 | 5 | 20 | 10 | – |
| 3(b)–(d) | 20 | 5 | 20 | 10 | – |
| 3(c) | 10 | – | 40 | 20 | (30,0.01) |
| 3(e) | 10 | 5 | – | – | (30,0.01) |
| 3(f) | 10 | 5 | – | – | (30,0.01) |

HF band, since the ratio $\sigma_z/\lambda_0$ is much smaller than one, the surface is slightly rough. From the Elfouhaily spectrum, Bourlier et al. [28] showed that the standard deviation of the height is $\sigma_z \approx 6.29 \times 10^{-3} u_{10}^{2.02}$. For instance for $u_{10} = 10\,\text{ms}^{-1}$ (Beaufort scale 6–7), $\sigma_z = 0.63\,\text{m}$, which implies that the ratio $\sigma_z/\lambda_0 \in [0.021; 0.042]$ for $f \in [10; 20]$ MHz.

By using a spectral method, several independent surfaces (but with the same Gaussian process and the same height spectrum) are generated. For each surface numbered $p$, the field $\psi_p$ and its normal derivative $\partial\psi_p/\partial n_s$ are computed, and then from Equations (9), (11) and (12), the scattered field $\psi_{s,p}$ and the function $F_p$ are computed. The average of $F$, denoted as $\langle F \rangle$, is then obtained from

$$\langle F \rangle = \frac{1}{N_r} \sum_{p=1}^{p=N_r} F_p, \tag{14}$$

where $N_r$ is the number of realizations.

From an asymptotic perturbative theory and assuming a *homogeneous flat* (no islands and the Earth's curvature is neglected) rough surface, Ishimaru et al. [10] showed that the coherent attenuation function $\langle F \rangle$ retains the same form as that of a smooth surface, but with a new surface normalized impedance, $\Delta^{\text{rough}}$, as functions of the smooth surface normalized impedance, $\Delta^{\text{flat}} = \Delta$, and of the sea roughness spectrum. In other words, $\Delta^{\text{rough}} \approx \Delta^{\text{flat}}(1 + a + jb)$, where $(a, b) \in \mathbb{R}^2$.

Assuming a *homogeneous flat* rough sea surface, Bourlier et al. [5] compared $a$ and $b$ with those obtained from an analytical approach developed by Barrick [8,9] and also based on an asymptotic perturbative theory. Good agreement is then obtained between both methods.

To our knowledge, the approach developed for a *homogeneous flat* rough surface has not been generalized to the case of an *inhomogeneous curved* rough surface. That is why, in references [5,7], this approach was tested for *homogeneous curved* and *inhomogeneous flat* rough surfaces, respectively. Then, good agreement was obtained between the intuitive approach (an analytical approach valid for a *flat* surface combined with Barrick's work to take the roughness into account) and the benchmark approach (BMIA-CAG or FB-SA). The proposed method is called

12                                    *C. Bourlier and G. Kubické*
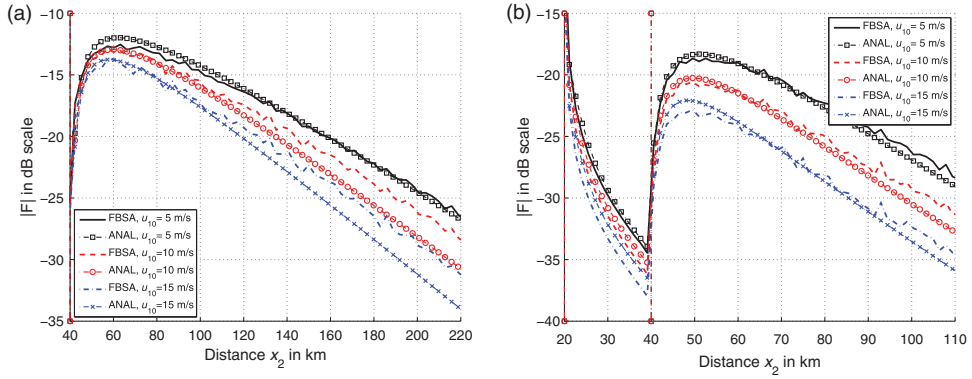


Figure 4. $|F|$ versus the horizontal distance $x_2 = x - x_0$ in km for an inhomogeneous curved rough surface. The simulation parameters are $h_1 = 0$ m, $w_1 = 20$ km, $x_1 = 30$ km, $(\epsilon_{r2}, \sigma_2) = (30, 0.01$ S/m$)$, $(\epsilon_{r1}, \sigma_1) = (\epsilon_{r3}, \sigma_3) = (80, 4$ S/m$)$ (sea), $z_0 = 10$ m, $x_0 = 0$ and $z = 5$ m. In addition, the number of realizations is $N_r = 10$. Top: $f = 10$ MHz; bottom: $f = 20$ MHz.

"intuitive" because it is not rigorous and it is rather based on a heuristic approach.
The purpose of this subsection is to test it.

Figure 4 plots the modulus of the attenuation function, $|F|$, versus the horizontal distance $x_2 = x - x_0$ in km for an inhomogeneous curved rough surface. The simulation parameters are listed in the figure caption. In sub figures 4(a) and (b) the $x$- and $y$-scales differ to better see the differences. Indeed, in Figure 4(a), the $x$-axis starts at 40 km and in Figure 4(b) at 20 km. Below these limits, the roughness effect is minor. As the roughness (or the wind speed) increases, $|F|$ decreases and the difference can reach 5 dB in comparison to a smooth surface, not shown here (for $f = 10$ MHz, see Figure 3(f) with $x_f = 40$ km). For $u_{10} = 0$ m s$^{-1}$, the results (not shown here) are the same as those computed for $u_{10} = 5$ m s$^{-1}$ within 0.5 dB. For $f = 20$ MHz, the intuitive approach matches well with the benchmark one, whereas for $f = 10$ MHz, the comparisons are less good. This behavior might seem strange because as the frequency decreases the roughness decreases and then the small perturbation method should work well. But, bear in mind that the intuitive approach is heuristic. In conclusion, the intuitive approach predicts satisfactory results (it underestimates the levels) and for a better prediction, further investigations must be conducted analytically.

### 4.3. *Smooth sea and different island shapes*

In this subsection, an inhomogeneous smooth sea surface is considered and $h_1 \neq 0$. In the FB-SA algorithm, the strong interaction distance is $x^{\text{FBSA}} = 300\lambda_0$.

Figure 5(a)–(d) plot the modulus of the attenuation function, $|F|$, versus the horizontal distance $x_2 = x - x_0$. For each figure, the simulation parameters are reported in Table 2. The numerical results are only computed from the FB-SA, since the analytical approach assumes that the island height vanishes. In Figure 5(a), the island shape changes and Figure 5(b) plots the same variation but versus $x_2$ and also
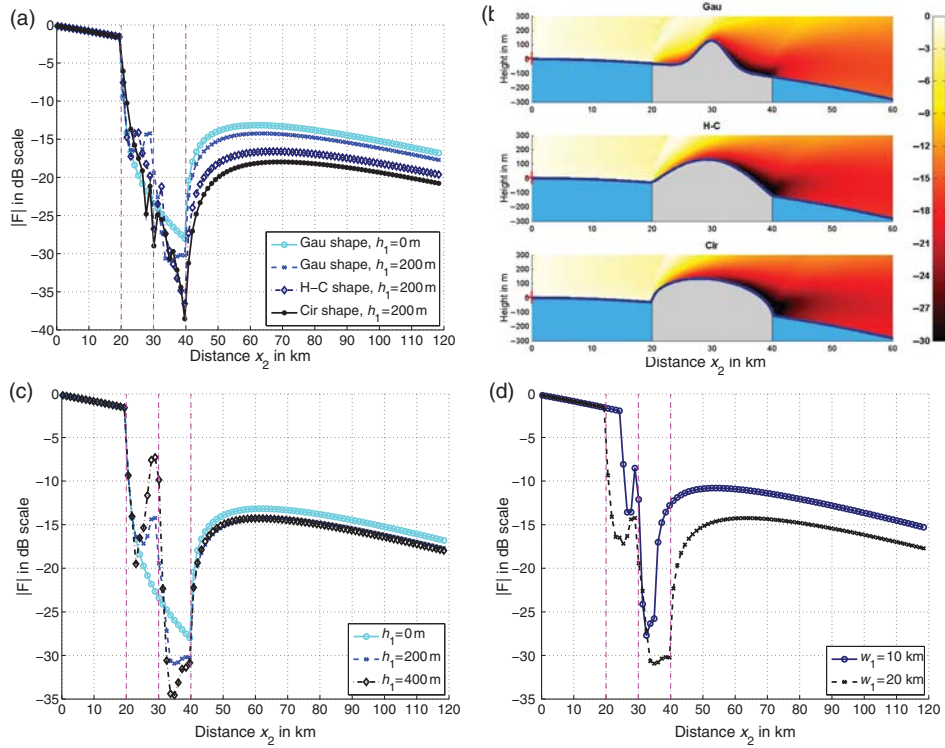
Figure 5. $|F|$ versus the horizontal distance $x_2 = x - x_0$ in km (and the receiver height $z$ for 5(b)) for an inhomogeneous curved smooth surface and computed from the FB-SA. The parameters are given in Table 2. The dashed vertical lines indicate the values of the abscissa at the beginning ($x_d$) and at the end ($x_f$) of the island.

Table 2. Parameters used for Figure 5(a)–(d). The wind speed is $u_{10} = 0$ (smooth sea surface), $\epsilon_{r1} = \epsilon_{r3} = 80$, $\sigma_1 = \sigma_3 = 4$ S/m, $(\epsilon_{r2}, \sigma_2) = (30, 0.01)$ S/m (island), the height of the emitter is $z_0 = 10$ m, its abscissa is $x_0 = 0$ m and the height of the receiver is $z = 5$ m. The symbol "–" means that the corresponding parameter changes in the figures.

| Figure | $f$ (MHz) | Shape | $x_1$ km | $w_1$ km | $h_1$ m |
|---|---|---|---|---|---|
| 5(a)–(b) | 10 | – | 30 | 20 | 200 |
| 5(c) | 10 | Gau | 30 | 20 | – |
| 5(d) | 10 | Gau | 30 | – | 200 |

315   the receiver height. Three shapes of islands are considered: a Gaussian (label "Gau"), a half-cosinusoidal (label "H-c") and a circular shape (label "Cir") defined from Equation (13). In Figure 5(c), the island height changes and in Figure 5(d), the island width changes.

14                          *C. Bourlier and G. Kubické*

320 As we can see in Figure 5(a) and (b), the attenuation function depends on the island shape. Above the island, the ground wave is strongly diffracted as the front slope increases, then near the back slope part the signal strength vanishes, which explains why the scattered field above the last path (sea) is smallest for a circular shape. For a Gaussian shape, the slope transition between the first and the second path is weak. Then, the recovery effect depends on the island shape and it is related
325 to the change of curvature between the first and second paths.

In Figure 5(c), as the maximum height of the island increases, the scattered field increases in the first part (front slope) of the island (accumulation of the scattered field), whereas the contrary behavior appears on the second part (back slope) of the island. Over the last path, the recovery effect is weakly related to $h_1$. In Figure 5(d),
330 as the island width increases, the signal strength decreases more rapidly over the island and then, over the last path, the signal strength decreases as the island width increases.

It is difficult to do a direct comparison with the results of [4] because the widths of the islands are smaller than 750 m and the horizontal distance $x$ did not exceed
335 40 km for a single island. In addition, the authors presented the path loss instead of the attenuation function. Nevertheless, comparing Figure 5(a)–(d) with those of [4], similar behavior is obtained.

## 5. Conclusion

For a vertically polarized line source in the HF band, the ground wave propagation
340 over one-dimensional highly conducting curved rough sea surfaces in the presence of islands (sea–land–sea mixed paths) was analyzed with an efficient rigorous numerical method: the method of moments combined with the FB-SA approach. In addition, the numerical results are compared with the Feinberg analytic solution. This is expressed in terms of a residue series and is valid for an inhomogeneous curved
345 *smooth* surface of parabolic profile. To include the sea surface roughness, the surface normalized impedance is substituted for a modified surface normalized impedance, which depends on the roughness spectrum and is computed with the Barrick model. In addition, the island height is assumed to be zero and the emitter and receiver heights are taken into account from the "height gain function" concept, which is a
350 heuristic approach.

For a smooth surface with zero island heights and zero receiver heights, comparisons then showed good agreement between the FB-SA results and the Feinberg results, which validates the analytical approach. On the other hand, for non-zero receiver heights, above the land path, the Feinberg approach predicts poor
355 results.

For a rough surface with zero island heights and zero receiver heights, the intuitive approach (the Feinberg formulation combined with the Barrick method to include the roughness) gives satisfactory results and the modulus of the attenuation function is underestimated compared to that computed from the FB-SA. In addition,
360 as the frequency increases, the comparisons are better. Simulations also showed that

the island shape, its width and its maximum height have an impact on the ground wave propagation against the same island with zero height.

This paper has demonstrated that the FB-SA method is a powerful tool for computing the attenuation function, but although this method is efficient in terms of computing time and memory storage, it cannot be applied to real-time applications. Indeed, for a number of unknowns equal to $\{100,000; 80,000; 150,000\}$ (Subsections 4.1, 4.2 and 4.3, respectively), the computing time to calculate the currents on the surface is approximately $\{1.0; 3.5; 3.4\}$ hours with $x^{\text{FBSA}} = \{50, 300, 50\}\lambda_0$ and requires approximately $4\,\text{GB}$ of memory with the MatLab software package. A personal computer with a $3.0\,\text{GHz}$ processor was used. In contrast, the intuitive approach only requires 5 seconds. Thus, further investigations should be carried out to improve and generalize the intuitive approach to more complex scenarios.

## References

[1] R.E. Collin, *Hertzian dipole radiating over a lossy Earth or sea: Some early and late 20th-century controversies*, IEEE Anten. Prop. Mag. 46 (2004), pp. 64–79.

[2] J.R. Wait, *The ancient and modern history of EM ground-wave propagation*, IEEE Anten. Prop. Mag. 40 (1998), pp. 7–39.

[3] L. Sevgi, *Ground wave modeling and simulation strategies and path loss prediction virtual tools*, IEEE Trans. Anten. Prop. 55 (2007), pp. 1591–1598.

[4] G. Apaydin and L. Sevgi, *Numerical investigations of and path loss predictions for surface wave propagation over sea paths including hilly island transitions*, IEEE Trans. Anten. Prop. 58 (2010), pp. 1302–1314.

[5] C. Bourlier, G. Kubické, and Y. Brelet, *Rigorous prediction of the ground wave above flat and rough highly-conducting one-dimensional sea surfaces in VHF band*, IEEE Trans. Anten. Prop. (2010), in press.

[6] C. Bourlier and G. Kubické, *HF ground wave propagation over a curved rough sea surface*, Waves Random Complex Media (2010), in press.

[7] C. Bourlier and G. Kubické, *Ground wave propagation along an inhomogeneous rough surface in the HF band: Millington effect for a flat Earth*, IEEE Trans. Geosci. Rem. Sensing (2010), in press.

[8] D.E. Barrick, *Theory of HF and VHF propagation across the rough sea, 1: The effective surface impedance for a slightly rough highly conducting medium at grazing incidence*, Radio Sci. 6 (1971), pp. 517–526.

[9] D.E. Barrick, *Theory of HF and VHF propagation across the rough sea, 2: Application to HF and VHF propagation above the sea*, Radio Sci. 6 (1971), pp. 527–533.

[10] A. Ishimaru, J.D. Rockway, Y. Kuga, and S.-W. Lee, *Sommerfeld and Zenneck wave propagation for a finitely conducting one-dimensional rough surface*, IEEE Trans. Anten. Prop. 48 (2000), pp. 1475–1484.

[11] L. Tsang, C.H. Chang, and H. Sangani, *A banded matrix iterative approach to Monte Carlo simulations of scattering of waves by large scale random rough surface problems: TM case*, Electron. Lett. 29 (1993), pp. 1666–1667.

[12] L. Tsang, C.H. Chang, H. Sangani, A. Ishimaru, and P. Phu, *A banded matrix iterative approach to Monte Carlo simulations of large scale random rough surface scattering: TE case*, J. Electromagn. Waves Appl. 29 (1993), pp. 1185–1200.

[13] N. Déchamps and C. Bourlier, *Electromagnetic scattering from a rough layer: Propagation-Inside-Layer Expansion method combined to an updated BMIA/CAG approach*, IEEE Trans. Anten. Prop. 55 (2007), pp. 2790–2802.

[14] D. Holliday, L.L. DeRaad Jr, and G.J. St-Cyr, *Forward–Backward: a new method for computing low-grazing angle scattering*, IEEE Trans. Anten. Prop. 44 (1995), pp. 1199–1206.

[15] H.T. Chou and J.T. Johnson, *A novel acceleration algorithm for the computation of scattering from rough surfaces with the Forward–Backward method*, Radio Sci. 33 (1998), pp. 1277–1287.

[16] D. Torrungrueng, J.T. Johnson, and H.T. Chou, *Some issues related to the novel spectral acceleration method for the fast computation of radiation/scattering from one-dimensional extremely large scale quasi-planar structures*, Radio Sci. 37 (2002), pp. 1–20.

[17] N. Déchamps and C. Bourlier, *Electromagnetic scattering from a rough layer: Propagation-Inside-Layer Expansion method combined to the Forward–Backward novel spectral acceleration*, IEEE Trans. Anten. Prop. 55 (2007), pp. 3576–3586.

[18] C. Bourlier, G. Kubické, and N. Déchamps, *A fast method to compute scattering by a buried object under a randomly rough surface: PILE combined with FB-SA*, J. Opt. Soc. Am. A 25 (2008), pp. 891–902.

[19] E.L. Feinberg, *Propagation of radio waves along an inhomogeneous surface*, Del Nuovo Cimento XI (1959), pp. 60–91.

[20] G. Millington, *Ground-wave propagation over an inhomogeneous smooth Earth*, Proc. Inst. Elect. Eng. 96 (1949), pp. 53–64.

[21] ITU-R, Recommendations, P-368-7, *Groundwave propagation curves for frequencies between 10 kHz and 30 MHz*, International Telecommunications Union, March 1992.

[22] L. Sevgi, *A mixed-path groundwave field strength prediction virtual tool for digital radio broadcast systems in medium and short wave bands*, IEEE Anten. Prop. Mag. 48 (2006), pp. 19–27.

[23] H. Bremmer, *Applications of operational calculus to ground-wave propagation, particularly for long waves*, IRE Trans. Anten. Prop. 6 (1954), pp. 267–272.

[24] J. Galejs, *Terrestrial Propagation of Long Electromagnetic Waves*, Pergamon Press, New York, 1972.

[25] N.A. Logan and K.S. Yee, *A mathematical model for diffraction by convex surfaces*, in *Electromagnetic Waves*, R.E. Langer, ed., University of Wisconsin Press, Madison, WI, 1962.

[26] J.R. Wait, *On the theory of propagation of electromagnetic waves along a curved surface*, Can. J. Phys. 36 (1958), pp. 9–17.

[27] T. Elfouhaily, B. Chapron, K. Katsaros, and D. Vandermark, *A unified directional spectrum for long and short wind-driven waves*, J. Geophys. Res. 102 (1997), pp. 781–796.

[28] C. Bourlier and G. Berginc, *Microwave analytical backscattering models from randomly rough anisotropic sea surface comparison with experimental data in C and Ku bands*, Prog. Electromag. Res. 37 (2002), pp. 31–78.